A Field Study of Pixel-Scale Variability of Raindrop Size Distribution in the Mid-Atlantic Region

*Ali Tokay**

Joint Center For Earth Systems Technology, University of Maryland Baltimore County and NASA Goddard Space Flight Center, Greenbelt, Maryland

Leo Pio D'Adderio

Department of Physics and Earth Science, The University of Ferrara, Ferrara, Italy

David B. Wolff and Walter A. Petersen

NASA Goddard Space Flight Center, Wallops Flight Facility, Wallops Island, Virginia

Submitted to Journal of Hydrometeorology

August 13, 2015

* Corresponding author's address:

NASA Goddard Space Flight Center, Code 612.0

Greenbelt, MD 20771

tokay@umbc.edu

Abstract

The spatial variability of parameters of raindrop size distribution and its derivatives is investigated through a field study where collocated PARSIVEL^2 and two-dimensional video disdrometers are operated at six sites in Wallops Island, Virginia from December 2013 to March 2014. The three-parameter exponential function is employed to determine the spatial variability across the study domain where the maximum separation distance was 2.3 km. The nugget parameter of exponential function is set to 0.99 and the correlation distance (d_0) and shape parameter (s_0) are retrieved minimizing root-mean-square error, after fitting it to the correlations of physical parameters. Fits were very good for almost all fifteen physical parameters. The retrieved d_0 and s_0 were about 4.5 km and 1.1, respectively, for rain rate (RR) when all twelve disdrometers were reporting rainfall with a rain rate threshold of 0.1 mm h^{-1} in one-minute observations. The d_0 decreased noticeably when one or more disdrometers were required to report rain. The d_0 was considerably different for a number of parameters (e.g. mass weighted diameter) but was about the same for the other parameters (e.g. RR) when rainfall threshold was reset to 12 dB for Ka-band and 18 dB for Ku-band reflectivity following the expected Global Precipitation Measurement mission's space-borne radar minimum detectable signals. The reduction of the database through elimination of a site did not alter d_0 as long as the fit was adequate. The correlations of 5-minute rain accumulations were lower when disdrometer observations were simulated for a rain gauge at different bucket sizes.

47 1. Introduction

48

49 The National Aeronautics and Space Administration (NASA) Global Precipitation
50 Measurement (GPM) mission aims to retrieve the three dimensional hydrometeor
51 size distribution of precipitation through its Dual-frequency Precipitation Radar
52 (DPR) on board the GPM core satellite (Hou et. al. 2014). The retrieval algorithm
53 outputs parameters of gamma model size distribution for each range bin utilizing
54 Ka- and Ku-band radar measurements (Seto et al. 2013). The lowest clutter free
55 range bin near the surface at nadir incidence is approximately 5 km radius and 125
56 m height. One of the key uncertainties of retrieved size distributions is its spatial
57 variability within a given DPR footprint. The spatial variability is a result of
58 precipitation gradient within the range volume, which may not be completely
59 covered by the precipitation. This variability contributes to Non-Uniform Beam
60 Filling (NUBF) which results in a higher degree of uncertainty in microwave sensor
61 based precipitation estimates where the instantaneous field of view is typically
62 bigger than the DPR footprint (Tokay et al. 2014a).

63

64 Scanning radars in range height indicator mode provides the most relevant data
65 source to study the spatial variability of hydrometeor size distribution in the
66 vertical, while gridded radar data at 1x1 km or 2x2 km resolution is a common
67 resource for studying the horizontal spatial variability. The parameters of the size
68 distribution that are derived from radar measurements are based on empirical
69 relationships (Bringi et al. 2004). There is also an uncertainty within the radar pixel

as its size increases away from radar. Disdrometers are an alternative resource for estimating the horizontal spatial variability but are associated with point sampling and it is quite costly to populate a dense network with disdrometers to sample the area of a satellite footprint. Therefore, there have been relatively few field studies conducted to determine the spatial variability of hydrometeor size distributions and all of these dealt with rainfall.

As part of the NASA's Tropical Rainfall Measurement Mission (TRMM) Ground Validation program, a number of impact type Joss-Waldvogel disdrometers were first deployed during a series of field campaigns and also deployed later at the NASA Wallops Flight Facility on Wallops Island, Virginia. The latter operation allowed for determination of the measurement accuracy of the disdrometers when six units were side-by-side (Tokay et al. 2005) and the spatial variability of raindrop size distribution (DSD) when three units were deployed across the Wallops Island strip, where the minimum and maximum separation distances were 0.65 and 1.7 km, respectively (Tokay and Bashor 2010). Later, four disdrometers were distributed across the same strip where the minimum and maximum separation distances were 0.4 and 5.0 km, respectively (Schröer 2011). The three-parameter exponential function was tested to determine the spatial variability of DSD and integral rain parameters. Since four disdrometers provide six pairs of correlations across 5 km, the fitted exponential function was subject to noticeable error.

92 Measurement accuracy is one of the key uncertainties in determining the spatial
93 variability of DSDs quantitatively. Each disdrometer type has its own shortcomings
94 in measuring the DSD, and comparative field studies where different types of
95 disdrometers were collocated, help quantify the uncertainties of the disdrometers
96 (Krajewski et al. 2006, Thurai et al. 2011, Tokay et al. 2013, 2014b). Indeed, the
97 Miriovsky et al. (2004) pioneer study was unable to determine the spatial variability
98 of reflectivity within 1 km^2 due to uncertainties of four different types of
99 disdrometers. Lee et al. (2009), on the other hand, used four Particle Occurrence
100 Sensor System (POSS) to study the spatial variability of DSD in stratiform rain
101 events. An S-band dual polarization radar scanned over the POSS units and the
102 spatial correlation of rainfall was higher in radar than in POSS especially at 15 and
103 30 km. This could partly be due to the differences between the sampling volumes of
104 the instruments.
105
106 The first comprehensive field study to quantify the spatial variability of the DSD was
107 conducted in Central Spain where eight dual PARSIVEL (PARticle Size VELocity)
108 disdrometers were deployed (Tapiador et al. 2010). The availability of number of
109 disdrometers allowed 28 pairs of correlations where the distances range from 0.2
110 km to 3.2 km. The dual units were aligned in both North-South and East-West
111 directions, and one of the five events had significant differences in correlations of
112 reflectivity between North-South and East-West aligned disdrometers. Jaffrain et al.
113 (2011), on the other hand, analyzed 53 hours of 16 PARSIVEL observations to
114 determine the spatial variability of DSD in a radar pixel (about 1 x 1 km^2) in

115 Lausanne, Switzerland. They concluded that the coefficient of variations for the
116 mass weighted diameter (D_{mass}), total concentration (N_T), and rain rate (RR) were
117 high and could not be explained solely by the uncertainty of the measurement.
118 Jaffrain and Berne (2012, JB12 hereafter) used the same set up of instruments to
119 determine the spatial variability of D_{mass}, N_T, and RR using a variogram analysis.
120 They reported that the variability was greater in convective rain than transitional
121 and frontal rain. They also noted a decreasing variability with decreasing temporal
122 resolution. Perhaps, the main issue of these studies is the measurement accuracy of
123 the PARSIVEL disdrometer. The low-cost laser resulted in overestimation of large
124 drops due to an inhomogeneous beam (Thurai et al. 2011, Tokay et al. 2013). The
125 manufacturer upgraded the PARSIVEL disdrometer with PARSIVEL^2 in 2011 (Tokay
126 et al. 2014b).
127
128 In contrast to disdrometers, rain gauges are low-cost, durable, easy to maintain and
129 are frequently deployed to adjust or validate radar rainfall estimates during either
130 two-month long field studies or longer-term field observations. Thus, rain gauge
131 networks are an excellent resource to study the spatial variability of rainfall (Habib
132 and Krajewski 2002, Gebremichael and Krajewski 2004, Ciach and Krajewski 2006,
133 among others). The spatial variability of rainfall is often quantified applying a three-
134 parameter exponential function to the corrections between the paired gauge
135 measurements. The parameters of the exponential function differs from one study
136 to another due to the differences in quality of rain gauge data, inter-gauge distances,
137 sample size, experiment period and location (Villarini et al. 2008). Logistics may

limit the inter-gauge distances, while long-term observations with dual or multiple gauge at each site has a clear advantage for a larger sample size and continuous gauge record at a given gauge site. The long-term observations also allow investigation of season-to-season differences in the spatial variability of rainfall. Tokay et al. (2014a), for instance, used five years of continuous rain gauge measurements in the Southern Delmarva Peninsula and showed that weather systems dominate spatial variability over a season. Nor'easters, for instance, dominate winter precipitation in the Mid-Atlantic region.

As a comparative study, the spatial variability of rainfall was quantified through X-band radar and rain gauge network (Moreau et al. 2009). The correlations between the paired radar pixels at 1 km^2 resolution were significantly higher than those between paired gauges underneath the radar pixel up to 8 km. The differences in correlations are attributed to the differences in sampling volume, while the errors in radar rainfall estimate and time-height ambiguity also be played a role. Another comparative study of the spatial variability of rainfall was conducted using S-band dual-polarization radar and 2DVD measurements during Mid-latitude Continental Convective Clouds Experiment (MC3E) (Bringi et al. 2015). A good agreement was found between the radar and disdrometer based spatial variability for RR, median volume diameter, and logarithmic normalized intercept parameter with respect to liquid water content (N_W) in a long lasting stratiform event. The correlation distances were lower in a relatively short convective event than the stratiform event for all three parameters.

161

162 This study investigates the pixel-space variability of DSD and integral rain
163 parameters employing a disdrometer network at NASA Wallops Flight Facility
164 (WFF), Wallops Island, Virginia (37.9 degree N and 75.4 degree W). The manuscript
165 is organized as follows: The disdrometer network and the database are presented in
166 Section 2. Section 3 introduces the three-parameter exponential function while the
167 parametric form of the DSD is given in Section 4. The probability and cumulative
168 distributions of the DSD and rain parameters can be found in Section 5. Section 6
169 depicts the spatial variability of DSD and rain parameters, while the sensitivity
170 studies are in Section 7. The conclusions are given in the last section.

171

172 2. Field Study

173

174 The disdrometer network consists of six sites where each site had one two
175 dimensional video disdrometer (2DVD) and one PARSIVEL^2 disdrometer. The sites
176 were distributed across WFF where the minimum and maximum separation
177 distances were 0.5 and 2.3 km, respectively (Figure 1a). One of the sites (Pad)
178 hosted a variety of tipping and weighing bucket rain gauges including two pit gauges
179 (Figure 1b). Another site was collocated with the Wallops Automated Surface
180 Observing System (ASOS) as well as additional tipping bucket rain gauges (Figure
181 1c). Table 1 summarizes the locations and distances between the sites.

182

PARSIVEL^2 is the third generation of the laser-optical PARSIVEL disdrometer (Tokay et al. 2014b). It is designed to measure the size and fall velocity of individual hydrometeors across its laser beam and is also present weather sensor. For rain, PARSIVEL outputs drop counts in a 32 x 32 size versus fall velocity matrix at selected time intervals ranging from 10-second to one-minute. The first two size bins are empty due to low signal to noise ratio and the smallest measurable raindrop corresponds to 0.25 mm diameter. The width of the size bins increases with the size of raindrops from 0.125 mm for drops to 1.2 mm, to 0.25 for drops up to 2.5 mm, to 0.5 mm for drops up to 5 mm, and to 1.0 mm for the larger drops. Therefore, there is noticeable uncertainty in determining the maximum drop size of the DSD. Based on 2DVD observations, the largest raindrop ever recorded is 9.7 mm diameter (Gatlin et al. 2015). The 25th bin corresponds to 9-10 mm and was considered as the largest bin for rain. For fall velocity, PARSIVEL has a range from 0.05 to 20.8 m s^{-1}, covering fall speeds of all types of hydrometeors. For rain, the 26th bin corresponds to 8-9.6 m s^{-1}, and covers the expected range for terminal fall speeds of very large raindrops (Beard 1976). However, PARSIVEL^2 underestimates the fall velocity of raindrops by approximately 1 m s^{-1} with respect to the expected terminal fall speed of raindrops at around 1 mm diameter (Tokay et al. 2014b). The underestimation in fall velocity is also evident for larger drops but the difference between the mean PARSIVEL^2 and terminal fall speed decreases with increasing size. The manufacturer recognizes this matter as a software error and it is expected that the new generation of instruments will mitigate this issue (Kurt Nemeth, OTT PARSIVEL, *personal communication*, 2015).

206

207 The 2DVDs are the “compact” third generation and are composing of sensor unit and
208 indoor personal computer (Schönhuber et al. 2007). The third generation compact
209 version has the optical components firmly mounted with no need for re-alignment
210 by the user. The distance of the optical slits to the rim of the housing was also
211 reduced aiming to eliminate inhomogeneous filling of the measurement area in
212 windy conditions. The high-speed line-scan cameras provides better matching of
213 falling hydrometeors between the two planes that are nominally 6 mm apart. The
214 2DVD records the time stamp of each raindrop including its equivalent diameter, fall
215 velocity, and oblateness as well as the sampling area. Common interruption of data
216 occurs often due to non-meteorological items (e.g. leaves) in the sampling cross
217 section, which is the main shortcoming of the 2DVD.

218

219 The dataset for this study spanned from December 2013 through March 2014.
220 While PARSIVEL^2 disdrometers operated nearly continuous during the experiment
221 period, a number of 2DVD units failed to operate in a few rain events. The raw
222 outputs of PARSIVEL^2 and 2DVD observations were integrated to one-minute after
223 screening secondary and mismatched drops that fell outside ±50% of their terminal
224 fall speed (Tokay et al. 2013). Several rain/no-rain thresholds were then applied to
225 the one-minute observations. All thresholds required a minimum of 10 drops. The
226 minimum RR of 0.1 mm h^{-1} resulted in 447 one-minute samples when all twelve
227 disdrometers reported rainfall. Considering the minimum detectable reflectivity of
228 the GPM DPR, the Ku-band reflectivity (Z_{Ku}) of 18 dB and Ka-band reflectivity (Z_{Ka})

of 12 dB (Seto et al. 2013) are the other two thresholds used in this study. The minimum RR was 0.11 and 0.08 mm h^{-1} for Z_{Ka} > 12 dB and 0.16 and 0.30 mm h^{-1} for Z_{Ku} > 18 dB for 2DVD and PARSIVEL², respectively. The sample sizes were 445 and 278 for Z_{Ka} > 12 dB and Z_{Ku} > 18 dB, respectively. The sample of Z_{Ka} > 12 included twelve one-minute spectra that were not in the RR > 0.1 mm h^{-1} based sample.

3. Methodology

A three-parameter exponential function is employed to quantify the spatial variability of the DSD. It has been widely used to determine the spatial variability of rainfall through rain gauge and radar rainfall studies (Habib and Krajewski 2002, Gebremichael and Krajewski 2004, Ciach and Krajewski 2006, Villarini et al. 2008, Moreau et al. 2009, Tokay et al. 2014a). The Pearson correlation coefficient, r, is applied to the selected DSD and rain parameters that are derived from disdrometer measurements at distance d. The parametric form of exponential function is then expressed as

$$r = r_0 \exp\left[\left(-\frac{d}{d_0}\right)^{s_0}\right] \qquad (1)$$

where r_0 is the correlation of a selected parameter derived from collocated instruments and is known as the nugget parameter and ideally should be one. However, collocated gauge and disdrometer observations show that the nugget

parameter ranges between 0.90 and 0.99. The other parameters of the exponential function are not sensitive to changes in r_0 within this range (Schröer 2011, Tokay and Özturk, 2012). In this study, r_0 was set to 0.99. The correlation distance d_0, and the shape parameter s_0, are then derived through minimizing the root mean square error between the observed and derived correlations. As an initial guess, d_0 values of 1 to 300 km and s_0 values of 0.1 to 2.0 were given.

The d_0 decreases with increasing s_0 when the correlation coefficient is high (Figure 2). When the variability is investigated over a relatively small domain as in this study, the correlations of the selected DSD or rain parameters may not have a decreasing trend with distance. If the correlations were high, the best fit results in very high d_0 and this should not be interpreted independent of other exponential function parameters. The parameters of exponential function are valid within the maximum distance of the study domain (Tokay and Öztürk 2012).

4. Raindrop Size Distribution

The normalized gamma distribution function is adopted to determine the spatial variability of DSD parameters. The normalization was done with respect to N_T and liquid water content W (Tokay and Bashor 2010). The normalized intercept parameters with respect to total concentration, N_T^* and liquid water content, N_W are expressed as

$$N_T^* = \frac{N_T}{D_{mass}} \quad (2)$$

$$N_w = \frac{256}{\pi \rho_w} \frac{10^3 W}{D_{mass}^4} \quad (3)$$

where ρ_w is the density of water. D_{mass} is related to the slope, Λ and shape parameter, m of the complete gamma distribution as;

$$D_{mass} = \frac{4 + m}{\Lambda} \quad (4)$$

The normalized intercept parameters can then be calculated from observed spectra as well. The corresponding normalized gamma fitted distributions are expressed as:

$$N(D) = N_T^* f_1(m) \left(\frac{D}{D_{mass}}\right)^m \exp\left[-(4 + m)\frac{D}{D_{mass}}\right] \quad (5)$$

$$N(D) = N_w f_2(m) \left(\frac{D}{D_{mass}}\right)^m \exp\left[-(4 + m)\frac{D}{D_{mass}}\right] \quad (6)$$

where $f_1(m)$ and $f_2(m)$ are given as;

$$f_1(m) = \frac{(4 + m)^{m+1}}{\Gamma(m + 1)} \quad (7)$$

293

294 $$f_2(m) = \frac{6}{256}\frac{(4+m)^{m+4}}{\Gamma(m+4)} \quad (8)$$

295

296 To extract the shape parameter, $m(N_T^*)$, and $m(N_W)$, the rain rates that are calculated
297 from observed and fitted gamma distributions (e.g. equations 5 and 6) are
298 minimized. The formulations presented above follows the complete gamma
299 function where minimum and maximum drop size is assumed zero and infinity,
300 respectively. In reality, there is a minimum and maximum drop size (D_{max}) in a
301 population of drops and the incomplete gamma function is more appropriate
302 especially if the size spectra do not contain the large drops (e.g. narrow
303 distribution), but this is the beyond the scope of this study.

304

305 The GPM DPR algorithm has adopted the normalized gamma function as in equation
306 6 (Seto et al. 2013). Since the DPR algorithm employs dual frequency reflectivity
307 measurements to determine the three parameters of gamma function, there is an
308 interest in finding relations between the derived parameters. Williams et al. (2014)
309 suggested a power law relation between the standard deviation of D_{mass} (σ_{mass}) and
310 D_{mass}. Both variables are directly calculated from observed DSD and their ratio is a
311 sole function of shape parameter, $m(\sigma_{mass})$ following complete gamma function.

312

313 $$\frac{\sigma_{mass}}{D_{mass}} = \frac{1}{(4+m)^{0.5}} \quad (9)$$

5. Probability and Cumulative Distributions

This study investigates the spatial variability of seven DSD and eight integral rain parameters. The DSD parameters include D_{mass}, D_{max}, N_T^*, N_W, $m(N_T^*)$, $m(N_W)$, and $m(\sigma_{mass})$, while the rain parameters were W, RR, dual polarization parameters of horizontal reflectivity (Z_H), and differential reflectivity (Z_{dr}), reflectivity at W-band (Z_W), Z_{Ku}, Z_{Ka}, and dual frequency ratio (DFR = Z_{Ku}/Z_{Ka}). The Ka-, Ku-, and W-band reflectivities are calculated using Mie scattering for spherical particles, while dual-polarization parameters are calculated for S-band radar following Tokay et al. (2002). Table 2 presents the mean, standard deviation, median, and 5^{th} and 95^{th} percentage of 15 physical parameters. Both N_T^* and N_W have ranges of several order of magnitude and, hence logarithmic values of these two parameters are used in constructing probability and cumulative distributions.

Among many factors listed in the introduction, knowledge of the characteristics of the DSD and rainfall is essential for quantifying the spatial variability. Observed DSD lacking large drops but with abundant small drops will incur different spatial variability than a DSD with numerous large drops but fewer small drops. The spatial variability of rainfall, on the other hand, differs in the presence and absence of heavy rain. The probability and cumulative distributions of the DSD and rain parameters provide an insight on the characteristics of DSD and rainfall, and these

337 distributions should be included if a similar study is conducted with a different
338 dataset.
339
340 Figure 3 presents the probability and cumulative distributions of fifteen DSD and
341 integral rain parameters based on 2DVD and PARSIVEL^2 measurements, when all
342 twelve units were reporting rainfall. A very good agreement in midsize range
343 (diameter 1-3 mm) of 2DVD and PARSIVEL^2 size spectra reflects an excellent
344 agreement in probability and cumulative distributions of D_{mass} between the two
345 disdrometers (Figure 2a). D_{mass} mostly resided between 0.8 and 1.5 mm, peaking at
346 1 mm (Table 2). The binning of drop counts results in quantization error in size
347 measurements in PARSIVEL^2, which is quite significant for D_{max} since the larger bins
348 have wider widths. The probability distribution of D_{max} in PARSIVEL^2 therefore had
349 multiple modes, while the probability distribution of D_{max} in 2DVD was a unimodal
350 (Figure 3b). The cumulative distributions of D_{max} agreed well between the two
351 types of disdrometers and the median D_{max} was around 1.9 mm for both (Table 2).
352
353 PARSIVEL^2 is relatively more sensitive to small drops less than 0.5 mm diameter
354 than the 2DVD (Tokay et al. 2013, 2014b). N_T^* is very sensitive to the number of
355 small drops since their concentrations are much higher than larger drops. The
356 probability distribution of $\log(N_T^*)$ of 2DVD and PARSIVEL^2 show a wide range, but
357 the PARSIVEL^2 based distribution was shifted to the larger concentrations,
358 consistent with its sensitivity to small drops (Figure 3c). N_W is more sensitive to
359 midsize drops and therefore an agreement is expected between the 2DVD and

PARSIVEL^2 distributions. A general agreement is evident between the distributions of log(N_W) with a median 3.55, but the PARSIVEL^2 also had low percentages of log(N_w) less than 2.5 (Figure 3d).

The shape parameter of the gamma distribution is very sensitive to the method of derivation and has a wide range but was mostly between 0 and 14 with mean and median around 5 (Table 2). While the agreement between 2DVD and PARSIVEL^2 derived distributions of shape parameters were reasonable for m(N_T^*) m(N_W), and m(σ_{mass}), the probability distribution of m(N_T^*) was shifted toward larger values in PARSIVEL^2 and m(N_W) and m(σ_{mass}) had slightly larger values in 2DVD (Figures 3e-g). The differences in probability and cumulative distributions are more pronounced in m(N_T^*) reflecting the differences in distributions of log(N_T^*).

An excellent agreement was evident in the distributions of W, and RR between the two different types of disdrometers (Figures 3h-i). Both W and RR are primarily sensitive to midsize drops, while the upper end of the small drops (0.8-1.0 mm) and the lower end of the large drops (3.0-4.0 mm) contribute to W and RR significantly in the presence of light and heavy rainfall, respectively. The mean and median RR is 1.1 and 0.9 mm h^{-1}, respectively (Table 2), indicating the dominance of light rain. Good agreement was also evident in distributions of Z_H, Z_{dr}, Z_W, Z_{Ku}, Z_{Ka}, and DFR between the two types of disdrometers (Figures 3j-o). The median Z_H, Z_{Ku} and Z_{Ka} were in the 22-23 dB range, while 95th percentiles were in the 31-32 dB range (Table 2) in the presence of widespread frontal rainfall.

383

384 6. Spatial Variability

385

386 The correlations of D_{mass} and D_{max} are higher for 2DVD than for PARSIVEL^2 at a given
387 distance (Figures 4a-b). PARSIVEL^2 based correlations were 0.55-0.7 for five paired
388 observations resulting in a higher RMSE. The quantization error due to binning
389 contributed to the low correlations in PARSIVEL^2 based D_{max}. The correlations of
390 N_T^* and N_W were higher than 0.9 for all distances for the 2DVD and decreased
391 gradually with distance (Figures 4c-d). PARSIVEL^2 based correlations have a wider
392 range than 0.1 at a given distance but remained higher than 0.84 and the RMSE was
393 quite low for fitted exponential function. The correlations of shape parameters
394 decreased with distance from 0.8 to 0.5 for $m(N_T^*)$ and from 0.8 to 0.4 for $m(N_W)$
395 and $m(\sigma_{mass})$ for both 2DVD and PARSIVEL^2 (Figures 4e-g). The range of
396 correlations was less than 0.1 at a given distance for both disdrometers resulting in
397 low RMSE. The sample size was 74% and 77% of the database for $m(N_T^*)$ and
398 $m(N_W)$, respectively due to the fact that the shape parameter was outside the
399 expected range of -4 to 20 for a number of size spectrum when normalized gamma
400 function was fitted minimizing rain rate. Similarly, the sample size was 76% of the
401 database for $m(\sigma_{mass})$ due to presence of shape parameters larger than 20. The
402 large shape parameters results from narrow size spectrum in the absence of large
403 drops. The shape of size spectrum exhibits more than a single peak with a plateau
404 in midsize regime for collisional break-up dominated DSD (D'Adderio et al. 2015).

405 The gamma distribution is not the best mathematical fit in these conditions, but this
406 is beyond scope of this paper.
407
408 The correlations of RR and W decreased with distance from 0.9 to 0.55 and from
409 0.92 to 0.64, respectively (Figures 4h-i). The spread in correlation between the
410 same and different types of disdrometers was much less than 0.1 at a given distance
411 resulting in very low RMSE. Thus, the exponential fits were nearly identical for both
412 types of disdrometers. The correlations of reflectivities at different wavelengths
413 decreased with distance but there were noticeable differences and similarities
414 among them. The correlations of Z_H and Z_{Ku} were about the same at a given distance
415 for a given disdrometer while the spread in PARSIVEL^2 derived correlations of Z_{Ka}
416 were less resulting in lower RMSE (Figures 4j, 4m-n). The spread in correlations of
417 Z_W were much less (less than 0.05) at a given distance for both disdrometer types
418 resulting in an excellent fit (Figure 4l). For Z_{dr}, there were significantly lower
419 correlations (0.35-0.55) for five PARSIVEL^2 pairs resulting in high RMSE (0.14)
420 (Figure 4k). For 2DVD, Z_{dr} decreased with distance and had a spread of 0.1 at a given
421 distance resulting in a reasonable fit with low RMSE. DFR, which is another
422 reflectivity ratio, had lower correlations even at short distances and the spread in
423 correlations were as high as 0.3 at a given distance in PARSIVEL^2 resulting in
424 relatively poor fit with high RMSE (0.12) (Figure 4o). For 2DVD, the fit was better
425 but the spread in correlation was 0.2 at a given distance.
426

427 The correlation distances were about the same for RR and W but higher in 2DVD
428 than in PARSIVEL^2 for the rest of rain and DSD parameters (Figure 5a). For N_T^* and
429 N_W, d_0 was at around upper limit of initial guess due to high correlations for all
430 distances. The d_0 was 4.2 and 4.5 km in RR in PARSIVEL^2 and 2DVD, respectively.
431 These correlation distances correspond to high spatial variability following gauge-
432 based studies (Ciach and Krajewski 2006). However, the correlations remained
433 high (> 0.7) in this study (Figure 4i). The gauge studies were conducted for 5-
434 minute or longer integration periods while high temporal scale in this study results
435 in higher variability even in the presence of lighter rain. The shape parameter, on
436 the other hand, remained between 0.4 and 1.0 for most of the fits (Figure 5b). The
437 RMSE was less than 0.08 for almost all parameters showing the goodness of fit
438 (Figure 5c). It should be emphasized that three-parameter exponential function is
439 applied for the first time for a number of DSD and rain parameters following
440 feasibility study (Schröer 2011). Therefore, there is no direct comparison available
441 for these parameters of exponential function with any other studies.
442
443 7. Sensitivity Studies
444
445 a) Disdrometer network availability
446
447 It is not uncommon that one or more disdrometers fail to operate throughout a field
448 campaign. For spatial variability, it is important to assess the goodness of fit of the
449 three-parameter exponential function when one of the sites is not available. In that

regard, five out of six sites were employed to quantify the sensitivity of parameters of exponential function to D_{mass} and RR. The elimination of a site reduced paired correlations from 15 to 10 and if site 5 or site 6 in Table 1 were not functioning, the maximum separation distance would be reduced to 1.84 km.

Fits were very good for 2DVD derived D_{mass} and RR regardless of the choice of elimination of paired correlations. The d_0 had a very narrow range of 4.2-4.7 km for RR but remained mostly within 11-21 km for D_{mass} (Figure 6a). For PARSIVEL^2, fits were good for RR but quite poor for D_{mass} repeating previous finding in Figure 4a. The d_0 had a wide range in PARSIVEL^2 derived D_{mass} but was not sensitive to the elimination of any paired correlation in RR. The s_0 was less than 1.0 and highly variable due to elimination of paired correlation in D_{mass} but remained mostly above 1.0 with almost no sensitivity to the elimination of paired correlation in RR (Figure 6b). The RMSE was 0.03 or less for 2DVD for both D_{mass} and RR but was higher than 0.1 for four trials for PARSIVEL^2 derived D_{mass} (Figure 6c).

b) Rain/No-rain threshold

The rain/no-rain threshold results in differences in the sample size and the distribution of the DSD and rain parameters. The higher sensitivity DPR footprint where Z_{Ka} is larger than 12 dB is expected to have less spatial variability with higher d_0 than the lower sensitivity DPR footprint where Z_{Ku} is larger than 18 dB. As shown in the gauge based study of Tokay and Özturk (2012), the higher thresholds

473 eliminate the light rain or low reflectivity samples and results in lower correlations,
474 especially if there is no precondition where both disdrometers must report rainfall.
475
476 Based on 2DVD observations, d_0 of D_{mass} was the lowest and the highest for Z_{Ku} and
477 RR thresholds, respectively (Figure 7a). The d_0 of RR and W was the same for RR
478 and Z_{Ka} thresholds and slightly lower for Z_{Ku} threshold. The d_0 of Z_{Ka}, Z_{Ku}, and Z_H
479 were about the same for Z_{Ka} and Z_{Ku} thresholds, and were lower than RR threshold.
480 The d_0 of DFR was the same for all three thresholds, while the other DSD and rain
481 parameters showed different trends. The shape parameter of exponential function
482 showed little or no variability when d_0 was about the same for given thresholds
483 (Figure 7b). The RMSE did not show significant differences between the different
484 thresholds for most of the DSD and rain parameters except for Z_{dr} and DFR where
485 RMSE was noticeably higher for Z_{Ku} threshold (Figure 7c).
486
487 c) Rain coverage
488
489 Partial coverage of satellite footprint or radar pixel by rain is one of the sources of
490 NUBF and contributes significantly to the spatial variability. To quantify the spatial
491 variability in the presence of partial coverage, PARSIVEL^2 observations were
492 reprocessed when all units were reporting rainfall and when at least one unit
493 reporting rainfall. The latter is more commonly observed in nature. The sample
494 size is 4,645 one-minute size distributions for the latter condition, which makes it
495 more than 2.6 times of the sample size of the former condition. The difference is

496 mainly due to the rain intermittence. The sample size when all six PARSIVEL^2
497 reported rainfall was 4 times larger than that when all twelve disdrometers
498 reported rainfall.
499
500 The correlation distance was distinctly lower for almost all physical parameters
501 when one or more PARSIVEL^2 reported rainfall (Figure 8a). It should also be noted
502 that d_0 was different from earlier findings when all six PARSIVEL^2 were reporting
503 rainfall. The bigger sample included more uniform rainfall across the study domain
504 and d_0 of RR was 14 km. The s_0 was higher when one or more PARSIVEL^2 reported
505 rainfall (Figure 8b). Fits were good for both conditions for physical parameters
506 except for normalized intercept and shape parameter of the gamma distribution
507 where fit was relatively poor with RMSE of 0.1 or higher (Figure 8c).
508
509 d) Rain gauge simulation
510
511 Tipping bucket rain gauges are widely used in precipitation studies but suffer from
512 significant sampling errors over short integration periods depending on the bucket
513 size (Habib et al 2001). A bucket size of 0.01 inch (0.254 mm) is used in ASOS
514 network but the gauge manufacturers also provide gauges with bucket resolutions
515 of 0.1 mm and 0.2 mm. The gauge based spatial variability of rainfall studies
516 employs 5-minute or longer integration periods to mitigate the sampling errors.
517

518 PARSIVEL^2 and 2DVD one-minute rain rate time series were employed to simulate
519 the time of tip for 0.1 mm, 0.2 mm, and 0.254 mm bucket resolutions. The
520 simulation study ignored any disdrometer malfunctions throughout the experiment
521 period. The 5-minute rainfall was then calculated from one-minute disdrometer
522 and three different simulated gauge datasets. The nugget parameter of 0.99 was
523 considered in all simulations. The correlations decrease noticeably with the size of
524 the bucket at a given distance in both PARSIVEL^2 and 2DVD based simulations
525 (Figure 9a-b). The decrease in correlations was gradual for disdrometer but quite
526 sharp for coarser relation bucket size based simulations from nugget to short
527 separation distances. At 2 km separation distance, the differences in correlations
528 were approximately 0.2 between disdrometer and 0.254 mm bucket simulations of
529 2DVD and PARSIVEL^2.
530
531 8. Conclusions
532
533 The pixel-scale variability of seven DSD and eight integral rain parameters was
534 investigated through a *unique* set of disdrometer observations where collocated
535 2DVD and PARSIVEL^2 were operated at six sites across the main base of NASA/WFF.
536 A three-parameter exponential function was employed to quantify the spatial
537 variability. The r_0, or nugget parameter, was fixed to 0.99 and d_0 and s_0 were
538 retrieved minimizing RMSE following fitting an exponential function to the
539 correlations that were derived from 2DVD or PARSIVEL^2 observations. The
540 correlations were calculated during periods when all twelve disdrometers reported

541 rainfall and a minimum RR threshold of 0.1 mm h^{-1} was satisfied with a minimum of
542 10 drops occurring in one-minute.
543
544 The there parameter exponential function is a simple mathematical form that
545 expresses the observed correlations well. It converged rapidly for almost all
546 physical parameters where RMSE was mostly less than 0.08. Very good agreement
547 between the 2DVD and PARSIVEL^2 derived correlations boosted our confidence in
548 the quality of the observations. The 2DVD outperformed the PARSIVEL^2 for
549 sampling of D_{max}, while the reverse was true for N_T^*. This is likely due to the
550 difference in the sensitivity of the respective disdrometers to the small and large
551 drop end of the size spectrum.
552
553 Given the confidence in measurement quality and fitting method, d_0 and s_0 should
554 mainly be sensitive to the characteristics of the DSD. The exclusion of a site did not
555 change the distribution of rainfall resulting in insignificant changes in d_0 and s_0 of
556 RR. The retrieved parameters of exponential function fits quite different in
557 PARSIVEL^2 derived D_{mass} when one site was removed but this is attributed to the
558 poor fitting. The d_0 and s_0 were sensitive to the different rain/no-rain thresholds.
559 They were also sensitive to the differences in conditions where one or more and all
560 six PARSIVEL^2 were reporting rainfall. The differences in the sample of
561 observations play a key role for differences in d_0 and s_0. The disdrometers have a
562 clear advantage to the rain gauges when spatial variability was studied for short
563 time intervals. The larger the bucket size the lower the correlations when the

564 disdrometer observations were used to simulate rain gauge observations at
565 different bucket size.
566
567 This is the first study where the three-parameter exponential function has been
568 used for estimating the variability of 15 physical parameters. Previously, JB12 used
569 the exponential function for RR. Their study was more robust in terms of the
570 number of available instruments and a longer period of observation. The
571 correlations decreased more rapidly for the first 500 m reaching 0.8 in JB12 study.
572 This study did not have any paired correlation in this short distance regime and the
573 correlation of RR was about 0.9 at 500 m. The differences in correlations are
574 attributed to the nature of rain. JB12 study included higher rainfall intensities than
575 this study.
576
577 The logistics often dominate the experiment set up and therefore the minimum and
578 maximum distances in the study domain. The sample size and type of rainfall play a
579 crucial role in quantifying the spatial variability. WFF is ideal site since rainfall from
580 multiple weather systems falls in all around year. In this study, light rain was
581 persistent throughout field study where mean RR was 1.1 mm h^{-1} and the 95^{th}
582 percentile of D_{max} was 3.1 mm (2DVD). For future studies, the larger domain where
583 the maximum disdrometer distance exceeds the DPR footprint and the combination
584 of light and heavy rain is desirable for quantification of spatial variability of DSD.
585 The limited but unique data set from Mid-latitude Continental Convective Clouds

586 experiment from Northern Oklahoma may prove to be a great resource for such a
587 follow-up study.
588
589 Acknowledgements
590
591 The authors are grateful to the NASA Wallops Precipitation Facility team, Matthew
592 Wingo, Katherine (Rhonie) Wolff, Paul G. Bashor, and Jason C. Bashor, for their
593 efforts on maintaining the disdrometer network. Discussion with Robert Meneghini
594 of NASA Goddard Space Flight Center (GSFC) was very helpful. This study was
595 partly conducted during second authors' visit to the NASA GSFC. The funding for the
596 second author's visit was provided through Federico Porcu of the University of
597 Bologna, Italy. This study was funded through NASA Precipitation measurement
598 mission grant NNX10AJ12G and funding from the Global Precipitation Measurement
599 Mission.
600
601 References
602
603 Beard, K. V., 1976: Terminal velocity and shape of cloud and precipitation drops
604 aloft. J. Atmos. Sci., 33, 851-864.
605
606 Bringi, V. N., R. Rang, and V. Chandrasekar, 2004: Evaluation of a new
607 polarimetrically based Z-R relation. J. Atmos. Oceanic. Technol., 21, 612-623.
608

609 Bringi, V., L. Tolstoy, M. Thurai, and W. Petersen, 2015: Estimation of spatial
610 correlation of rain drop size distribution parameters and rain rate using NASA's S-
611 band polarimetric radar and 2D-video disdrometer network: Two case studies from
612 MC3E. J. Hydrometeor. doi:10.1175/JHM-D-14-0204.1, in press.
613
614 Ciach, G. J., and W. F. Krajewski, 2006: Analysis and modeling of spatial correlation
615 structure of small-scale rainfall in Central Oklahoma. Adv. Water Resour., 1450-
616 1463.
617
618 D'Adderio, L. P., F. Porcu, and A. Tokay, 2015: Raindrop size distribution in the
619 presence of break-up. J. Atmos Sci. (accepted for publication).
620
621 Gebremichael, M., and W. F. Krajewski, 2004: Characterization of the temporal
622 sampling error in space-time-averaged rainfall estimates from satellite. J. Geophys.
623 Research., 109, doi: 10.1029/2004JD04509.
624
625 Habib, E., W. Krajewski, and A. Kruger, A., 2001: Sampling Errors of Tipping-Bucket
626 Rain Gauge Measurements. J. Hydrol. Eng., 6(2), 159–166.
627
628 Habib, E., and W. Krajewski, 2002: Uncertainty analysis of the TRMM ground-
629 validation radar-rainfall products: Application to the TEFLUN-B field campaign. J.
630 Appl. Meteor., 41, 558-572.
631

632 Hou, A., R. Kakar, S. Neeck, A. A. Azarbarzin, C. D. Kummerow, M. Kojima, R. Oki, K.
633 Nakamura, and T. Iguchi, 2014: The global precipitation measurement mission. Bull.
634 Amer. Meteor. Soc., 95, 701-722.
635
636 Jaffrain, J., A. Studzinski, and A. Berne, 2011: A network of disdrometers to quantify
637 the small-scale variability of the raindrop size distribution. Water Resources Resea.,
638 47, W00H06, doi:10.1029/2010WR009872.
639
640 Jaffrain, J., and A. Berne, 2012: Quantification of the small-scale spatial structure o
641 fthe raindrop size distribution from metwork of disdrometers. J. Applied Meteor.
642 Climatol., 51, 941-953.
643
644 Moreau, E., J. tested, and E. Le Bouar, 2009: Rainfall special variability observed by
645 X-band weather radar and its implication for the accuracy of rainfall estimates. Adv.
646 Water Resour., 32, 1011-1019.
647
648 Schöenhuber, M., G. Lammer, and W. L. Randeu, 2007: One decade of imaging
649 precipitation measurement by 2D video disdrometer. Adv. Geosci., 10, 85-90.
650
651 Schröer, J-B, 2011: Spatial and temporal variability of raindrop size distribution.
652 Diploma Thesis. The University of Bonn, Bonn, Germany, 133pp.
653

654 Seto, S., T. Iguchi, and T. Oki, 2013: The basic performance of a precipitation
655 retrieval algorithm for the global precipitation measurement mission's single/dual-
656 frequency radar measurements. IEEE Trans. Geoscience Rem. Sensing, 51, 5239-
657 5251.
658
659 Tapiador, F. J., R. Checa, and M. de Castro, 2010: An experiment to measure the
660 spatial variability of raindrop size distribution using sixteen laser disdrometers.
661 Geophys. Res. Lett., 37, L16803, doi: 10.1029/2010GRL044120.
662
663 Thurai, M., W. A. Petersen, A. Tokay, C. Schultz, and P. Gatlin, 2011: Drop size
664 distribution comparisons between PARSIVEL and 2-D video disdrometers. Adv.
665 Geosci., 30, 3–9.
666
667 Tokay, A., A. Kruger, W. Krajewski, P. A., Kucera, and A. J. Pereira Filho, 2002:
668 Measurements of drop size distribution in the southwestern Amazon basin. *J.*
669 *Geophys. Res.*, **107**, D20, 8052, doi:10.1029.
670
671 Tokay, A., P. G. Bashor, and K. R. Wolff, 2005: Error characteristics of rainfall
672 measurements by collocated Joss-Waldvogel disdrometers. J. Atmos. Oceanic
673 Technol., 22, 513-527.
674
675 Tokay, A., and P. G. Bashor, 2010: An experimental study of small-scale variability of
676 raindrop size distribution. J. Hydrometeor., 11, 2348-2365.

677

678 Tokay, A., and K. Öztürk, 2012: An experimental study of the small-scale ariability of
679 rainfall. J. Hydrometeor., 13, 351-365.

680

681 Tokay, A., W. A. Petersen, P. Gatlin, and M. Wing, 2013: Comparison of raindrop size
682 distribution measurements by collocated disdrometers. J. Atmos. Oceanic Technol.,
683 30, 1672-1690.

684

685 Tokay, A., R. J. Roche, and P. G. Bashor, 2014a: An experimental study of spatial
686 variability of rainfall. J. Hydrometeor., 15, 801-812.

687

688 Tokay, A., D. B. Wolff, and W. A. Petersen, 2014b: Evaluation of the new version of
689 the laser-optical disdrometer, OTT PARSIVEL^2. J. Atmos. Oceanic Technol., 31, 1276-
690 1288.

691

692 Villarini, G., P. V. Mandapaka, W. F. Krajewski, and R. J. Moore, 2008: Rainfall and
693 sampling uncertaintites: A rain gauge perspective. J. Geophy. Resea., 113, doi:
694 10.1029/2007/JD009214.

695

696 Williams, C. R., V. N. Bringi, L. D. Carey, V. Chandrasekar, P. N. Gatlin. Z. S. Haddad, R.
697 Meneghini, S. J. Munchak, S. W. Nesbitt, W. A. Petersen, S. Tanelli, A. Tokay, A. Wilson,
698 and D. B. Wolff, 2014: Describing the shape of raindrop size distributions using

699 uncorrelated raindrop mass spectrum parameters. J. Applied Meteor. Climatol., 53,
700 1282-1296.
701
702
703

704 Figure Captions:

705

706 Figure 1. Google Map of six field sites at the NASA Wallops Flight Facility (top).
707 Picture of 2DVD, PARSIVEL^2 among other precipitation measuring instruments at
708 the Pad (middle) and at the Automated Surface Observing System site (bottom).
709 Please note that not all the instruments collecting data at the Pad during the
710 experiment period.

711

712 Figure 2. Dependence of the correlation distance to correlation coefficient at a given
713 distance and shape parameter when nugget parameter is set to 0.99. Four different
714 shape parameters and two different distances are used.

715

716 Figure 3. Probability and cumulative distributions of (a) mass weighted diameter,
717 (b) maximum diameter, (c) logarithmic normalized intercept parameter, N_T^*, (d)
718 logarithmic normalized intercept parameter, N_W, (e) shape parameter with respect
719 to N_T^*, (f) shape parameter with respect to N_W,, (g) shape parameter with respect to
720 σ_{mass}, (h) liquid water content, (i) rain rate, (j) horizontal reflectivity, (k) differential
721 reflectivity, (l) reflectivity at W-band, (m) reflectivity at Ku-band, (n) reflectivity at
722 Ka-band, (o) dual frequency ratio. Distributions of these physical parameters are
723 derived from 2DVD and PARSIVEL^2 observations.

724

725 Figure 4. Spatial variability of (a) mass weighted diameter, (b) maximum diameter,
726 (c) logarithmic normalized intercept parameter, N_T^*, (d) logarithmic normalized

intercept parameter, N_W, (e) shape parameter with respect to N_T^*, (f) shape parameter with respect to N_W,, (g) shape parameter with respect to σ_{mass}, (h) liquid water content, (i) rain rate, (j) horizontal reflectivity, (k) differential reflectivity, (l) reflectivity at W-band, (m) reflectivity at Ku-band, (n) reflectivity at Ka-band, (o) dual frequency ratio, all derived from 2DVD (blue dots) and PARSIVEL² (red stars) observations. The parameters of the three-parameter exponential function including root-mean-square error and the sample size are also given.

Figure 5. (a) Correlation distance and (b) shape parameter of the three-parameter exponential function and (c) root-mean-square error for fifteen physical parameters based on 2DVD (blue dots) and PARSIVEL² (red stars) observations. Several correlation distances were higher than y-axis range and are marked with their values.

Figure 6. Sensitivity of (a) the correlation distance, (b) shape parameter of the three-parameter exponential function and of (c) root-mean-square error of mass weighted diameter (left) and rain rate (right) to the elimination of a site (e.g. site1) during the experiment. Several correlation distances were higher than y-axis range and are marked with their values.

Figure 7. Sensitivity of (a) the correlation distance, (b) shape parameter of the three-parameter exponential function and of (c) root-mean-square error of fifteen physical parameters to the rainfall threshold following 2DVD observations. The

750 rainfall thresholds of Z_{Ka} > 12 dB (green dot), Z_{Ku} > 18 dB (black dot), and RR > 0.1 m
751 h^{-1} (red dot) are considered. Several correlation distances were higher than y-axis
752 range and are marked with their values.
753
754 Figure 8. Sensitivity of (a) the correlation distance, (b) shape parameter of the
755 three-parameter exponential function and of (c) root-mean-square error of fifteen
756 physical parameters to rain coverage. One or more (orange stars) as well as all six
757 (red stars) PARSIVEL^2 reporting rainfall was considered. Several correlation
758 distances were higher than y-axis range and are marked with their values.
759
760 Figure 9. Spatial variability of 5-minute rainfall derived from (a) 2DVD and (b)
761 PARSIVEL^2 observations (red), simulated gauge at 0.1 mm bucket (blue), simulated
762 gauge at 0.2 mm bucket (green), and simulated gauge at 0.254 mm bucket (black).
763
764

765 Table 1. NASA Wallops Flight Facility Precipitation Data Acquisition Network. The

766 distances between the six sites are given in km.

767

	Site #	Site 1	Site 2	Site 3	Site 4	Site 5	Site 6
	Site name	Pad	ASOS	Balloon Launch Facility	Building A41	Visitor Center	Water Treatment Plant
	Coordinates	37.944°N, 75.464°W	37.944°N, 75.481°W	37.938°N, 75.456°W	37.934°N, 75.471°W	37.929°N, 75.473°W	37.937°N, 75.466°W
Site 1			0.51	0.60	1.25	1.34	1.41
Site 2				1.06	1.81	0.88	1.53
Site 3					1.84	1.75	1.80
Site 4						0.99	1.52
Site 5							2.31

768

769

770 Table 2: Mean, standard deviation, median, and 5th and 95th percentiles of seven
771 DSD and eight integral parameters that were derived from 2DVD and PARSIVEL^2
772 (Par^2) observations.
773

DSD and integral rain parameters	mean		standard deviation		median		5th percentile		95th percentile	
	2DVD	Par^2	2DVD	Par^2	2DVD	Par^2	2DVD	Par^2	2DVD	Par^2
D_{mass} (mm)	1.11	1.09	0.30	0.32	1.05	1.01	0.72	0.72	1.64	1.63
D_{max} (mm)	2.03	1.96	0.58	0.63	1.92	1.93	1.28	1.22	3.07	3.35
N_T^* ($m^{-3}mm^{-1}$)	302	951	394	2,271	184	319	47	64	1,065	4,274
N_w ($m^{-3}mm^{-1}$)	6,524	7,313	9,294	10,915	3,468	3,588	711	53	26,787	32,706
$m(N_T^*)$	4.85	5.95	2.92	3.87	4.40	5.10	1.10	1.40	10.30	13.65
$m(N_w)$	5.16	5.00	3.38	4.01	4.50	4.00	0.80	0.10	11.40	12.90
$m(\sigma_{mass})$	5.75	5.41	3.54	4.18	5.23	4.60	0.90	-0.01	12.14	13.45
RR (mmh^{-1})	1.10	1.15	0.94	1.00	0.87	0.91	0.25	0.27	2.94	2.92
W (gm^{-3})	0.071	0.077	0.054	0.056	0.059	0.065	0.019	0.021	0.188	0.191
Z_h (dB)	26.4	27.7	18.0	33.4	22.3	22.1	15.0	15.0	31.2	31.8
Z_{dr} (dB)	0.376	0.394	0.291	0.427	0.287	0.273	0.119	0.112	0.839	0.938
Z_W(dB)	16.9	17.3	3.4	3.2	15.8	16.4	11.3	11.8	20.8	21.1
Z_{Ku} (dB)	26.8	27.7	18.5	22.1	21.9	21.7	14.8	14.7	31.7	32.7
Z_{Ka} (dB)	26.3	26.2	5.8	6.3	23.4	23.2	15.2	15.5	31.4	31.5
DFR	-0.99	-0.86	1.19	1.11	-1.27	-1.04	-2.04	-1.86	1.26	0.78

774
775
776

777

778 Figure 1. Google Map of six field sites at the NASA Wallops Flight Facility (top).
779 Picture of 2DVD, PARSIVEL² among other precipitation measuring instruments at
780 the Pad (middle) and at the Automated Surface Observing System site (bottom).
781 Please note that not all the instruments collecting data at the Pad during the
782 experiment period.
783
784

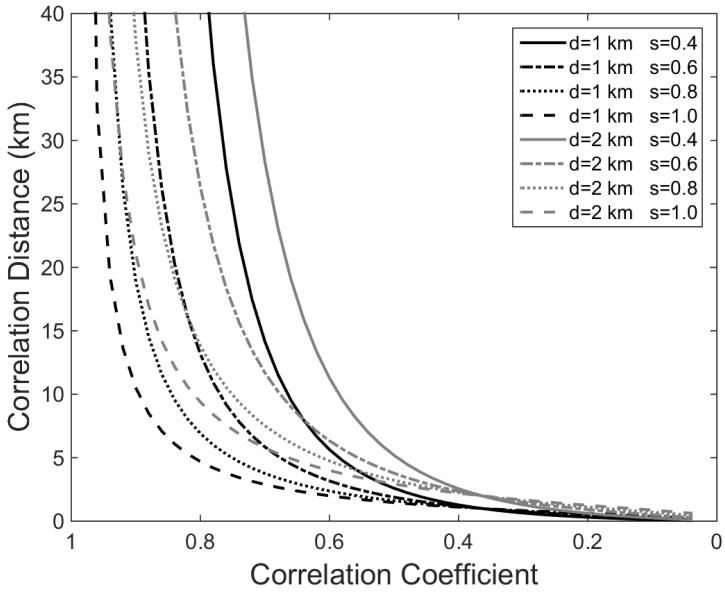

Figure 2. Dependence of the correlation distance to correlation coefficient at a given distance and shape parameter when nugget parameter is set to 0.99. Four different shape parameters and two different distances are used.

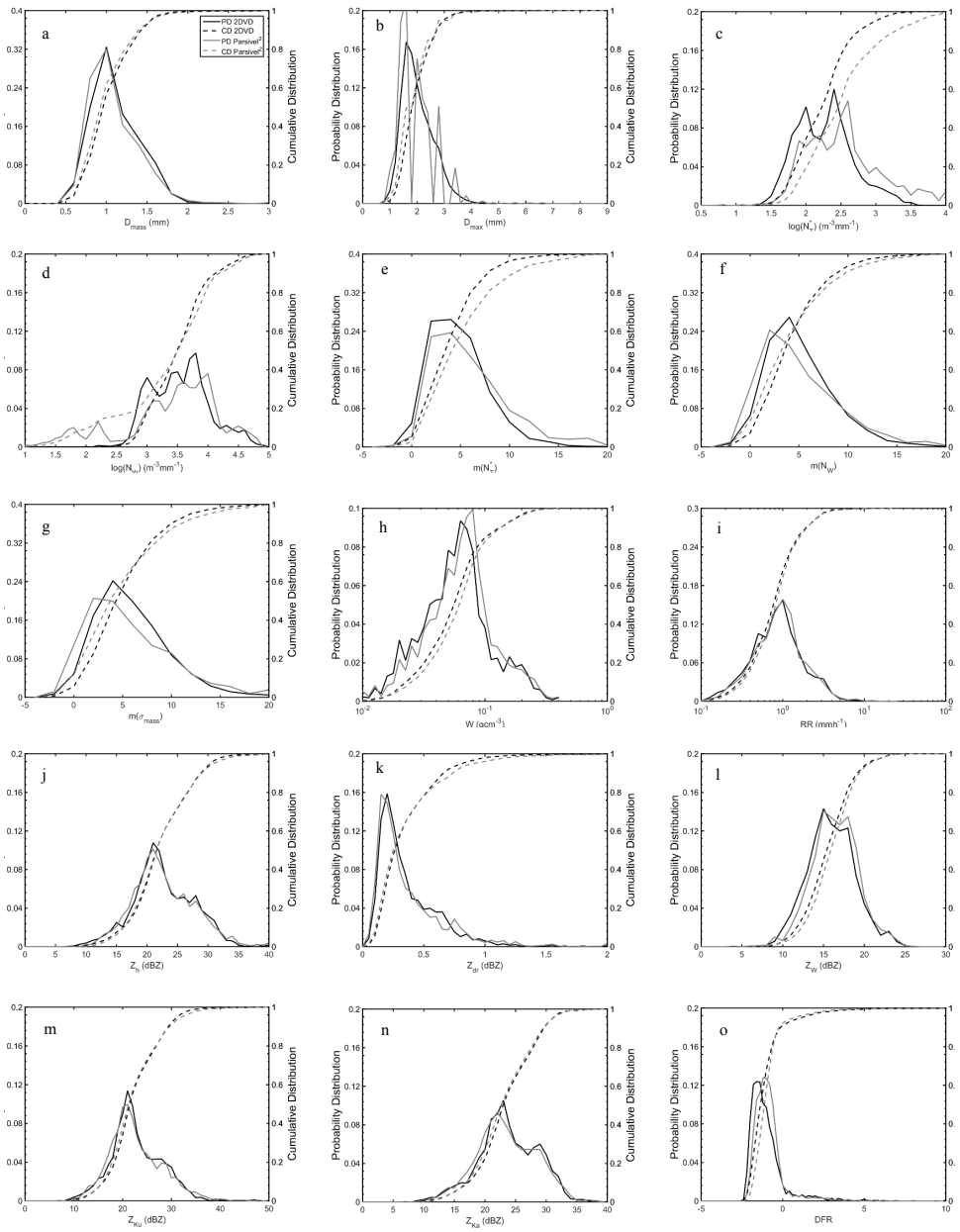

Figure 3. Probability and cumulative distributions of (a) mass weighted diameter, (b) maximum diameter, (c) logarithmic normalized intercept parameter, N_T^*, (d) logarithmic normalized intercept parameter, N_W, (e) shape parameter with respect to N_T^*, (f) shape parameter with respect to N_W, (g) shape parameter with respect to σ_{mass}, (h) liquid water content, (i) rain rate, (j) horizontal reflectivity, (k) differential reflectivity, (l) reflectivity at W-band, (m) reflectivity at Ku-band, (n) reflectivity at Ka-band, (o) dual frequency ratio. Distributions of these physical parameters are derived from 2DVD and PARSIVEL^2 observations.

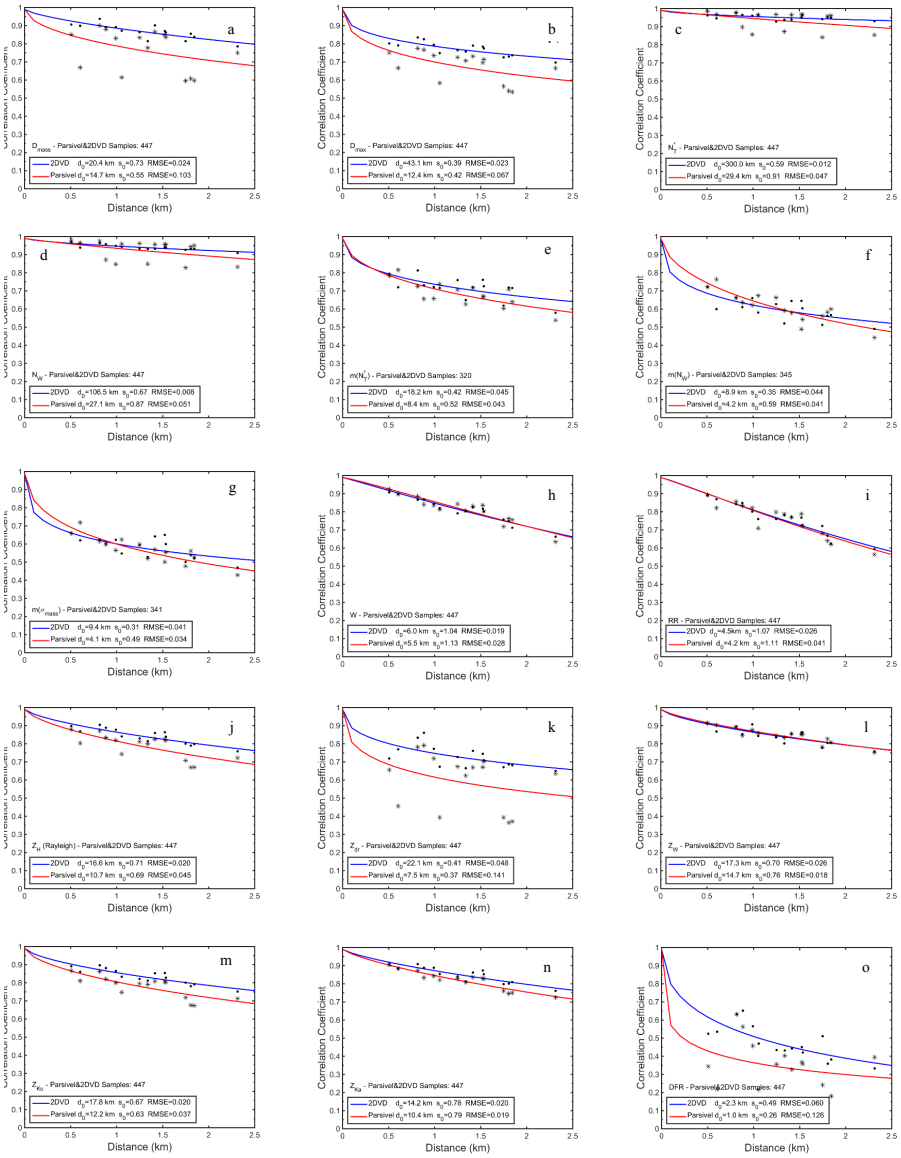

Figure 4. Spatial variability of (a) mass weighted diameter, (b) maximum diameter, (c) logarithmic normalized intercept parameter, N_T^*, (d) logarithmic normalized intercept parameter, N_W, (e) shape parameter with respect to N_T^*, (f) shape parameter with respect to N_W,, (g) shape parameter with respect to s_{mass}, (h) liquid water content, (i) rain rate, (j) horizontal reflectivity, (k) differential reflectivity, (l) reflectivity at W-band, (m) reflectivity at Ku-band, (n) reflectivity at Ka-band, (o) dual frequency ratio, all derived from 2DVD (blue dots) and PARSIVEL^2 (red stars) observations. The parameters of the three-parameter exponential function including root-mean-square error and the sample size are also given.

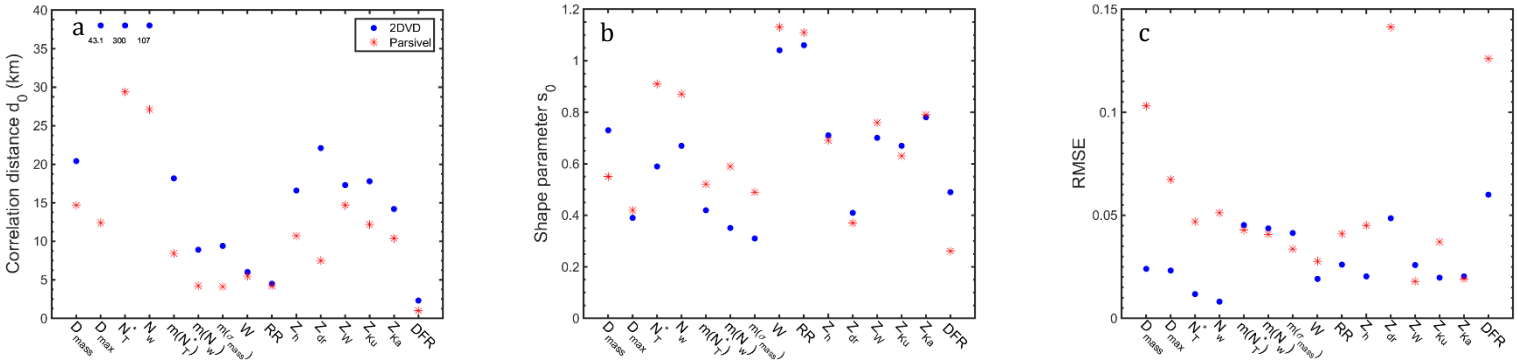

Figure 5. (a) Correlation distance and (b) shape parameter of the three-parameter exponential function and (c) root-mean-square error for fifteen physical parameters based on 2DVD (blue dots) and PARSIVEL² (red stars) observations. Several correlation distances were higher than y-axis range and are marked with their values.

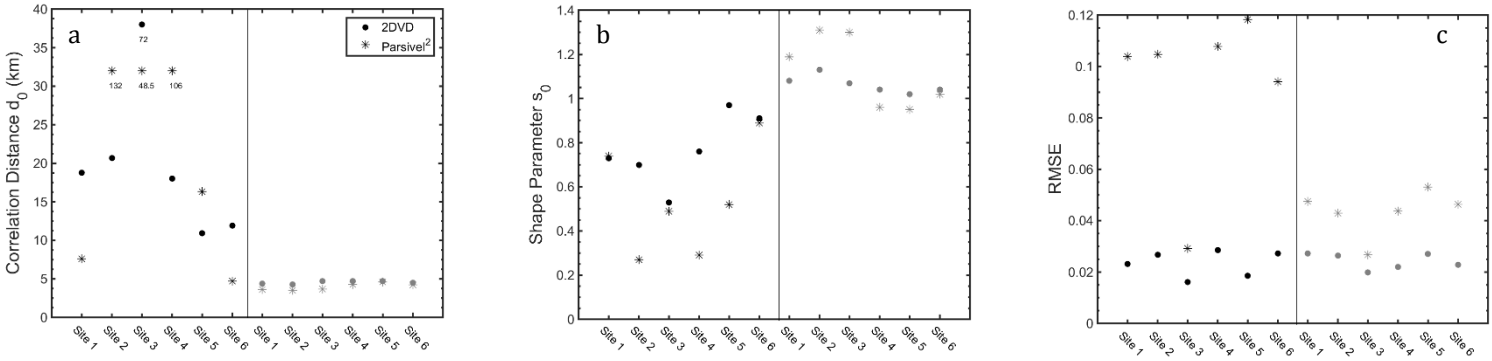

Figure 6. Sensitivity of (a) the correlation distance, (b) shape parameter of the three-parameter exponential function and of (c) root-mean-square error of mass weighted diameter (left) and rain rate (right) to the elimination of a site (e.g. site1) during the experiment. Several correlation distances were higher than y-axis range and are marked with their values.

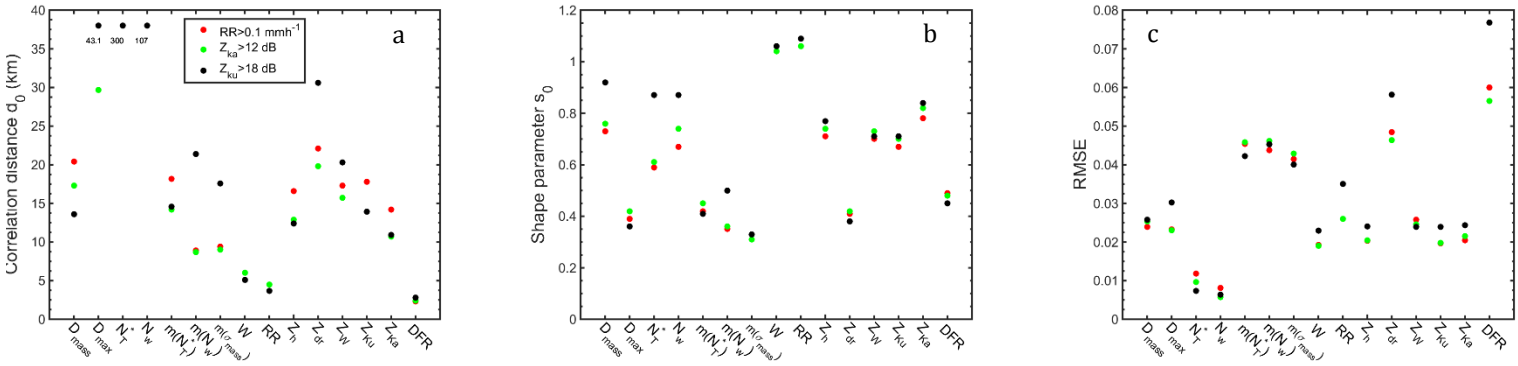

Figure 7. Sensitivity of (a) the correlation distance, (b) shape parameter of the three-parameter exponential function and of (c) root-mean-square error of fifteen physical parameters to the rainfall threshold following 2DVD observations. The rainfall thresholds of Z_{Ka} > 12 dB (green dot), Z_{Ku} > 18 dB (black dot), and RR > 0.1 m h^{-1} (red dot) are considered. Several correlation distances were higher than y-axis range and are marked with their values.

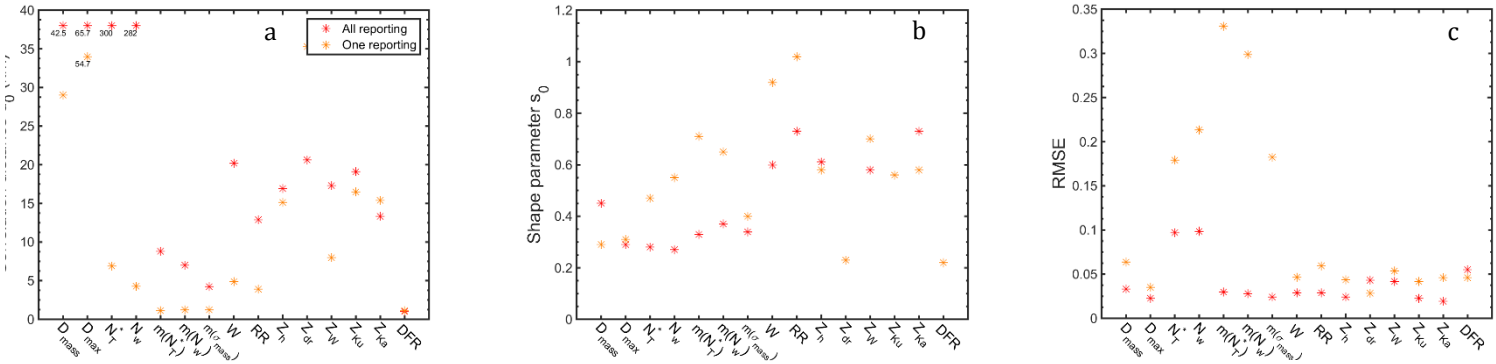

Figure 8. Sensitivity of (a) the correlation distance, (b) shape parameter of the three-parameter exponential function and of (c) root-mean-square error of fifteen physical parameters to rain coverage. One or more (orange stars) as well as all six (red stars) PARSIVEL² reporting rainfall was considered. Several correlation distances were higher than y-axis range and are marked with their values.

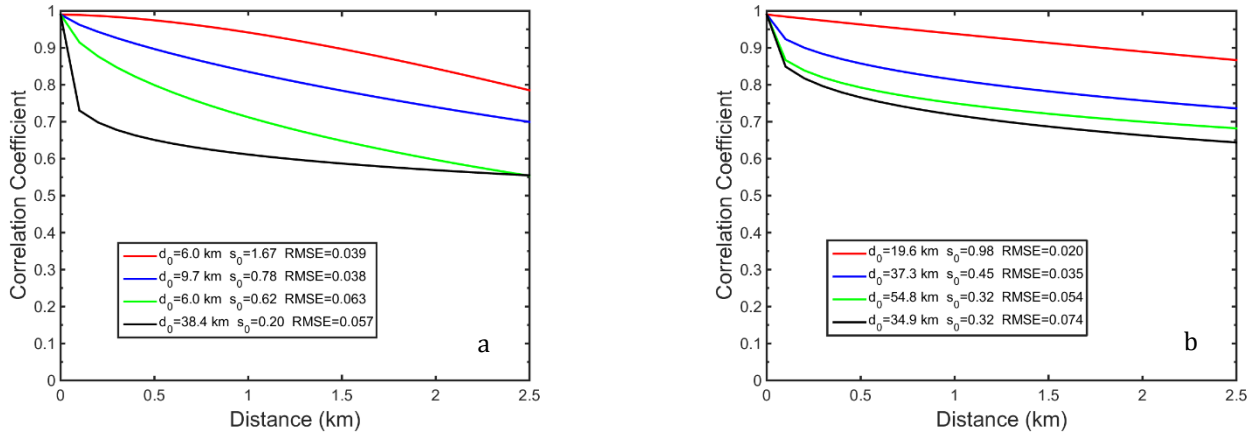

Figure 9. Spatial variability of 5-minute rainfall derived from (a) 2DVD and (b) PARSIVEL² observations (red), simulated gauge at 0.1 mm bucket (blue), simulated gauge at 0.2 mm bucket (green), and simulated gauge at 0.254 mm bucket (black).